Journal of Energetic Materials
Publication details, including instructions for authors and subscription information:
http://www.informaworld.com/smpp/title~content=t713770432

Jet initiation and penetration of explosives

Charles L. Mader[a]; George H. Pimbley[a]
[a] Los Alamos National Laboratory Los Alamos, New Mexico, USA

To cite this Article Mader, Charles L. and Pimbley, George H.(1983) 'Jet initiation and penetration of explosives', Journal of Energetic Materials, 1: 1, 3 — 44
To link to this Article: DOI: 10.1080/07370658308010817
URL: http://dx.doi.org/10.1080/07370658308010817

JET INITIATION AND PENETRATION OF EXPLOSIVES

Charles L. Mader and George H. Pimbley
Los Alamos National Laboratory
Los Alamos, New Mexico 87545 (USA)

ABSTRACT

The two-dimensional Eulerian hydrodynamic code 2DE, with the shock initiation of heterogeneous explosive burn model called Forest Fire, is used to model numerically the interaction of jets of steel, copper, tantalum, aluminum, and water with steel, water, and explosive targets.

The calculated and experimental critical condition for propagating detonation may be described by the Held V^2d expression (jet velocity squared times the jet diameter). In PBX 9502, jets initiate an overdriven detonation smaller than the critical diameter, which either fails or enlarges to greater than the critical diameter while the overdriven detonation decays to the C-J state. In PBX 9404, the jet initiates a detonation that propagates only if it is maintained by the jet for an interval sufficient to establish a stable curved detonation front.

The calculated penetration velocities into explosives, initiated by a low-velocity jet, are significantly less than for nonreactive solids of the same density. The detonation products near

Journal of Energetic Materials Vol. 1,003-044(1983)

Published in 1983 by Dowden, Brodman & Devine, Inc.

the jet tip have a pressure higher than that of nonreactive explosives, and thus slow the jet penetration. At high jet velocities, the calculated penetration velocities are similar for reactive and inert targets.

INTRODUCTION

One of the first detailed treatments describing how a metallic jet can be formed by imploding a metal cone or hemisphere, and the resulting jet penetration of a metal target, was that of Birkhoff, MacDougall, Pugh, and Taylor.[1] The process of initiation of explosives by copper jet penetration was investigated by Held,[2] who correlated observations using $V_j^2 d$, where V_j is the jet velocity and d is the jet diameter. The $V_j^2 d$ values at which copper jets just caused propagating detonation in various explosive targets have been called "critical values."

Studies of shock initiation by jets near the critical conditions contrast with other shock initiation studies. For the latter, if detonation occurred, it was because the initiating shock wave was of sufficient strength and duration to build up to detonation. The propagating detonation was assured by the large geometry. In near-critical jet initiation, however, a prompt detonation of the explosive results, which develops into a propagating detonation only if the shock wave produced by the jet is of sufficient magnitude and duration.

Penetration velocities of projectiles interacting with explosives initiated by the projectile are reported[3] to be much lower

than the penetration velocities in nonreactive solids of the same density.

Jets formed by a shaped charge with a metal cone contain small-diameter, high-velocity projectiles. They can be approximated by cylinders or balls of uniform velocity with the appropriate dimensions. Behind the tip of the jet, the velocity of the projectiles decreases.

If we assume that Bernoulli's theorem applies (that is, that the flow is steady, that the jet pressure is large compared to the target or jet material strengths, and that pressure is the same in the jet and target near the interface), then

$$\frac{1}{2}\rho_j(V_j - V_p)^2 = \frac{1}{2}\rho_t V_p^2 \quad .$$

Here ρ is density and V is velocity (subscript j implies jet, t implies target, and p signifies penetration). Rearranging this expression gives the velocity ratio

$$\frac{V_p}{V_j} = \frac{1}{1 + \sqrt{\rho_t/\rho_j}} \quad , \tag{1}$$

It is customary to call this use of Bernoulli's theorem the "ideal model."

Experimental data from many studies of jets penetrating inert targets indicate that Bernoulli's theorem gives a satisfactory approximation for the V_p/V_j ratio. For example, Johnson's[4] two-dimensional numerical calculations of copper jet penetration into

aluminum targets adhere rather well to this ideal model. However, the data and calculations by Rice[3] of ball penetration into PBX 9404 or Composition B deviate seriously from the ideal model. The measured penetration velocities were significantly less than predicted.

Our study examines jet and projectile penetration of both nonreactive solids and explosives by comparing calculated and experimental penetration. The object was that of understanding the underlying processes, particularly with reference to the failure of the ideal penetration model for explosives. The numerical modeling was performed using the Los Alamos 2DE Eulerian reactive hydrodynamic code with the shock initiation of heterogeneous explosive burn model called Forest Fire.[5]

STEEL JET PENETRATING STEEL

Two PHERMEX radiographs (shots 1181 and 1185) of a steel jet penetrating a steel block have been published.[6] The steel jet was formed by a 4.0-mm-thick steel hemishell driven by a 60.0-mm-thick PBX-9404 hemisphere. The jet interacted with a steel block after 308 mm of free run from the center of the hemisphere. The measured maximum velocity of the jet, 18 mm/μs, was at the jet tip. Back from the tip, the velocity decreased approximately 1.3 mm/μs for each 10 mm of length. The first radiograph was taken after the jet had penetrated 45 mm of steel in 6 μs with an average penetration velocity of 7.5 mm/μs. In the second radiograph, the jet had penetrated an additional 35 mm of steel in 7.0 μs with an

average penetration velocity of 5.0 mm/μs. The jet diameter was uncertain because of its diffuse irregular boundaries in the radiograph, but one can estimate the diameter as 8-12 mm.

This steel jet into steel experiment was modeled numerically so as to furnish a benchmark for evaluation of the calculations. Equation-of-state parameters used for 347 stainless steel were the same as given in Appendix B of Ref. 7. The steel shock Hugoniot was described by $U_s = 4.58 + 1.51\ U_p$, where U_s,U_p are, respectively, the shock and particle velocities. The initial density of the steel was 7.917 mg/mm^3 and the Grüneisen coefficient γ was 1.25. Elastic-plastic terms were negligible, and tension was permitted only in the target. The cell size for this calculation was 0.2 mm square.

The calculated density profiles, with the experimental shock front and interface from the radiographs superimposed, are shown in Figs. 1 and 2 after 6.0 and 13 μs, respectively. The experimentally observed jet penetration of the steel plate appears to be adequately reproduced by the calculations, including the space observed between the jet and target walls, and the splash wave. The observed agreement between the radiographs and numerical model suggests that the important features of jet penetration are being described, and that we are justified in exploiting our investigative technique further. To test the ideal penetration model, we will now simplify our jet to be a rod or sphere moving initially with a uniform velocity.

STEEL ROD PENETRATING STEEL

Having demonstrated that steel target penetration by a steel jet of decreasing velocity can be modeled numerically, we next examine the penetration physics of the simpler system of a 10-mm-diammeter steel rod (with uniform velocity) penetrating a steel block. In the numerical approximation, the computational mesh had cells that were 1-mm square. The time step was 4×10^{-3} μs. Two initial velocities were selected for the rod: 15 and 10 mm/μs.

Pressure and velocity near the upper tip of the rod are shown as functions of time in Fig. 3 for initial velocity of 15 mm/μs. Contours of pressure, density, energy, and velocity are shown in Fig. 4 at 8.0 μs. Events are similar for the 10-mm/μs rod and are shown below in parentheses.

The steel rod propelled at 15 mm/μs (10 mm/μs) sends an initial shock pressure of about 950 GPa (480 GPa) into the steel target, along with a 16-mm/μs (12.1 mm/μs) shock velocity and a 7.5-mm/μs (5.0 mm/μs) particle velocity. Radial motion of the steel target decreased the tip pressure to about 250 GPa (100 GPa), and the particle velocity remained at about 7.5 mm/μs (5.0 mm/μs). The shock wave was supported by the higher pressure at the rod-target interface.

These results are consistent with the following ideal penetration model. For a planar shock wave (conditions near the projectile tip at early times), the shock impedance expression is $V_j/V_p = 1 + \rho_t U_{st}/\rho_j U_{sj}$, where U_s is the shock velocity. For jets

and targets of the same material, $V_p = \frac{1}{2}V_j$ for both the initial shock match across the interface and for the later penetration after steady state is achieved (Eq. 1). The shock pressure decreases from $\rho_t U_{st} V_p$ to $\frac{1}{2}\rho V_p^2$, and the shock wave moves out into the target ahead of the rod-target interface with a speed similar to the penetration velocity of the rod.

TANTALUM ROD PENETRATION

To examine the effect of different materials on the penetration process, we modeled an unreported experiment performed by Campbell and Hantel at the Los Alamos National Laboratory.[8] The penetration velocity of the tantalum jet (V_j = 6.6 to 7.3 mm/μs) into a steel plate was 4.0 mm/μs. The tantalum shock Hugoniot was described by $U_s = 3.414 + 1.201\ U_p$, $\rho = 16.69$ mg/mm^3, and $\gamma = 1.4$. Two calculations were performed for 7.3- and 6.6-mm/μs tantalum rods. The calculated penetration velocities were 4.0 mm/μs and 3.7 mm/μs, respectively, in good agreement with the experiments.

We also calculated the penetration of tantalum rods in water, inert Composition B, and reactive Composition B. As predicted by the ideal model, a tantalum (ρ = 16.69 mg/mm^3) rod at a given initial velocity penetrates inert Composition B (ρ = 1.715 mg/mm^3) faster than it does steel, and penetrates water (ρ = 1.0 mg/mm^3) even faster. The ideal interface pressures and penetration velocities agree with the numerical results over a wide range of velocities and densities. The only exception in our studies was the case of reactive Composition B, where the penetrating velocity was

lower and the interface pressure was greater in the calculation than in the ideal model. See the compared nonreactive and reactive one-dimensional graphs of these pressures and velocities in Fig. 5.

We examine the reactive case in detail following the next section.

JET INITIATION OF EXPLOSIVES AND THE $\rho V^2 d$ CRITICAL CONDITION

In this section we discuss the general topic of the initiation of an explosive by projectiles of small diameter and high velocity.

An early investigator was Held,[2] who shot copper jets, formed by a shaped charge, through steel plates of varying thickness, and observed the velocities of the resulting exit projectiles by x-ray flash photography. These projectiles were then permitted to interact with an explosive, and the critical velocity necessary for initiation of propagating detonation was determined. He then observed that his data could be correlated by assuming that the critical quantity connected with this initiation was the velocity (V) of the projectile squared times the diameter (d). If the velocity is in millimeters per microsecond and the projectile jet diameter is in millimeters, he reported that the critical V^2d for copper jets initiating 60/40 RDX/TNT at 1.70 g/cc was about 5.8.

Similar experiments have been performed by A. W. Campbell at Los Alamos[8] for copper jets initiating PBX 9404 (94/3/3 HMX/nitrocellulose/Tris-β-chloroethyl phosphate at 1.844 mg/mm^3) and PBX

9502 (95/5 TATB/Kel-F at 1.894 mg/mm^3). Critical values of V^2d were 127 ± 5 $mm^3/\mu s^2$ for PBX 9502, 16 ± 2 $mm^3/\mu s^2$ for PBX 9404, 37 $mm^3/\mu s^2$ for 75/25 Cyclotol at 1.743 mg/mm^3, and 29 $mm^3/\mu s^2$ for Composition B-3 at 1.713 mg/mm^3.

The failure diameter of an unconfined explosive charge is that diameter below which a propagating C-J detonation cannot maintain itself. The failure diameter of PBX 9502 is 0.9 cm, while that of PBX 9404 is 0.12 cm. This large difference is a consequence of the shock initiation properties of these explosives, as discussed in Ref. (5), pp. 264-266.

If one performs the pressure-particle velocity match shown in Fig. 6 for copper at 5.0 mm/μs shocking inert PBX 9502, the pressure match is 680 kbar, and at 6.0 mm/μs the pressure match is 920 kbar. Because the C-J pressure of PBX 9502 is 285 kbar, the copper jet must initiate a strongly overdriven detonation. The projectile diameter (~4 mm) was less than half the failure diameter (9.0 mm) of unconfined PBX 9502.

Also shown in Fig. 6, the pressure match is 340 kbar for PBX 9404 being shocked by copper initially at 3.0 mm/μs and is 250 kbar at 2.5 mm/μs. The distance of run for PBX 9404 at 250 kbar (i.e., the distance that a shock, resulting from a 250-kbar impulse, travels to detonation in shock initiation) is about 0.5 mm, so propagating detonation would occur very quickly. The projectile diameter (~2 mm) is somewhat larger than the unconfined PBX 9404 failure diameter (1.2 mm).

These jet projectile experiments have been modeled numerically. In one set of calculations, a 2-mm-radius copper cylinder (V_j = 7 mm/μs) penetrating PBX 9502, was modeled using a mesh 0.2 mm square. The calculated profiles are shown in Figs. 7 and 8. The 5-mm/μs initial velocity case was also calculated.

The copper projectile initiates an overdriven detonation smaller than the critical diameter which enlarges to greater than the critical diameter of PBX 9502. When the PBX 9502 was shocked by the 5.0-mm/μs copper cylinder, the detonation was decayed by side and rear rarefactions before enlarging to the critical diameter.

The numerically obtained V^2d values given by these computations bracketed the Campbell experimental critical V^2d of 127 for copper projectiles. Further similar calculations were made for an aluminum cylinder and a water cylinder. The shock pressure sent into the explosive depends upon the material of the projectile, so the aluminum must have a greater velocity or diameter than the copper projectile to furnish an equivalent impulse to the PBX 9502. One then expects that the critical V^2d is larger for aluminum than for copper and larger still for a water projectile. These conclusions were confirmed by the calculations with the predicted V^2d for aluminum being 325 ± 75, and for water about 800. To first approximation, the PBX 9502 has a critical ρV^2d of 800.

Further computations were made of a copper cylinder of 1-mm radius being shot into PBX 9404 at 3 mm/μs and at 2 mm/μs. The

copper projectile initiates detonation which propagates only if it is maintained by the shock long enough to establish a stable curved detonation front. The numerical values of V^2d bracketed the experimental Campbell critical V^2d of 16 for copper projectiles initiating propagating detonation in PBX 9404. For aluminum and water projectiles, the critical calculated V^2d values were 60 ± 20 and 150 ± 50, respectively. The critical ρV^2d for PBX 9404 is approximately 150.

The V^2d criterion introduced above, and used by Held and Campbell, relates to a critical value above which a propagating detonation is produced in a given explosive when shocked by a projectile composed of a given material. We propose that a new ρV^2d critical condition would be more general. Here, V = velocity of the projectile, d = diameter of the projectile, and ρ = density of the material of the projectile. A critical value, CV, of ρV^2d (such that if $\rho V^2d > CV$, the explosive goes off, and does not go off otherwise) would be intrinsic for the explosive and substantially independent of the projectile material.

STEEL BALL PENETRATION OF EXPLOSIVES

The penetration velocity of a 13-mm-diameter steel ball, moving at various speeds and striking 25-mm-thick cylinders of PBX 9404 or Composition B, was reported by Rice.[3] We have modeled this system numerically, comparing the results with the experimental data of Frey.[3] The mesh size was 0.5416 mm by 0.5 mm, and the time step was 0.005 μs.

Figure 9 shows the experimental data and the calculated results for both PBX 9404 and Composition B targets. The ball velocity loss, plotted vertically, is defined as the initial ball velocity less the penetration velocity. The agreement between experimental and computational results shows that the model does describe the important processes of explosive penetration and initiation.

When the steel ball was penetrating inert or nearly inert explosive, the penetration velocity could be described by the ideal model. When the ball velocity was just sufficient to cause propagating detonation, however, both the observed and calculated penetration velocities were much lower than predicted by the ideal model. As the ball velocity was increased above the critical value for propagating detonation, the actual and ideal penetration velocities gradually drew closer together. See Fig. 9.

A plot of the interface pressure and velocity in the Z direction near the axis of the ball, as functions of time, for 1.0- and 1.2-mm/μs balls penetrating PBX 9404 is shown in Fig. 10. The faster ball causes prompt initiation of the PBX 9404, and the interface pressure is much higher, and velocity loss greater, than for the slower ball (which does not cause prompt initiation).

The critical ball velocity for PBX 9404 shown in Fig. 9 is 1.14 mm/μs. The $V_j^2 d$ for this explosive, for steel penetration, was 16.0; therefore, the ball has an effective diameter of 12.3 mm. The critical ball velocity for Composition B is 1.8

mm/μs. The $V_j^2 d$ for this explosive is 29; therefore, the ball has an effective diameter of 9.0 mm when shocking Composition B.

STEEL ROD PENETRATION OF EXPLOSIVES

The steel ball exhibits a complicated flow. It was desirable to examine a simpler system to test the ideal penetration model and to determine why the ideal model fails for explosives. Therefore, we replaced the ball by a steel rod of the same diameter, and rods with velocities of 2.0 and 6.0 mm/μs were calculated penetrating reactive and nonreactive Composition B. The interface pressures and velocities near the advancing upper tip of the steel rod, as functions of time, are shown in Figs. 11 and 12.

The lowered penetration velocity of a projectile moving into detonating (rather than inert) explosive is caused by the higher pressure at the projectile-detonation product interface. The ideal model assumes zero pressure at zero particle velocity, which is correct for nonreactive solids. For explosives the constant volume detonation pressure at zero particle velocity is approximately 10 GPa for a slab of Composition B. In diverging flow, the detonation product pressure at zero particle velocity is about 5 GPa. The effect is not included in the ideal model.

If we assume that the ideal model is appropriate for the steel rod, and if we set the calculated detonation product interface pressure (5.0 GPa for the 2.0-mm/μs rod) equal to $\frac{1}{2}\rho_j(V_j - V_p)^2$, we estimate a 0.9 mm/μs penetration velocity. This is close to the 1.0 mm/μs calculated.

The relative difference between the ideal penetration velocity and the calculated penetration velocity decreases with increasing projectile velocity. The ideal model improves at higher projectile velocities, where the difference between the explosive reactive and nonreactive pressures (of about 4 GPa) becomes insignificant. See Fig. 12.

We have also modeled a 16-mm-diam steel rod moving at velocities lower than those necessary for initiating propagating detonation (1.0 mm/μs) in PBX 9404, and at velocities great enough to penetrate the explosive faster than the detonation velocity (8.8 mm/μs). The study investigated the penetration velocity in explosives throughout the range of possible jet velocities and examined the steel rod and explosive interface pressure effect described in the previous section. It also determined what would occur if the penetration velocity were greater than the C-J detonation velocity.

The computational problem consisted of a rectangular array of cells, each 2 mm square. A time step of 0.008 μs was used in the calculation. A summary of the calculations is presented in Table I.

The interface or rod tip pressures and velocities as functions of time, for a steel rod with a 15-mm/μs initial velocity penetrating PBX 9404, are shown in Fig. 13. Pressure and mass fraction contours for this rod are shown in Fig. 14. The pressure, density, and velocity one-dimensional graphs along the z-axis are

TABLE 1. Steel Rod Penetrating PBX 9404

Initial Rod Velocity (mm/μs)	Final Calc. Penetration Velocity (mm/μs)	Ideal Penetration Velocity* (mm/μs)	Interface Pressure (GPa)	Ideal Interface Pressure** (GPa)	Diverging Effective C-J Pressure (GPa)	Detonation Velocity (mm/μs)	Comments
15.0	10.6	10.117	100	94.37	90	10	Steady overdriven detonation wave
13.0	9.2	8.768	75	70.89	60	8.8	Steady overdriven detonation wave
11.0	7.8	7.419	55	50.75	40	8.8	Decaying wave moving faster than rod
9.0	6.2	6.07	38	33.97	36	8.7	Diverging detonation wave moving faster than rod
8.0	5.5	5.396	31	26.84	35	8.7	Diverging detonation wave moving faster than rod
5.0	3.2	3.37	15	10.5	35	8.7	Diverging detonation wave moving faster than rod
3.0	1.8	2.02	8	3.77	35	8.7	Diverging detonation wave moving faster than rod
2.5	1.4	1.686	7	2.6	35	8.7	Diverging detonation wave moving faster than rod
2.0	1.1	1.35	6	1.7	35	8.7	Diverging detonation wave moving faster than rod
1.5	0.6	1.01	5	0.9	35	8.7	Diverging detonation wave moving faster than rod
1.0	0.25	0.67	5	0.4	35	8.7	Diverging detonation wave moving faster than rod
0.7	0.5	0.47	0	0.2	--	----	No detonation, decaying shock wave
0.5	0.36	0.34	0	0.1	--	----	No detonation, decaying shock wave
0.3	0.22	0.20	0	0.04	--	----	No detonation, decaying shock wave

*0.674 rod velocity.
**0.922 (penetration velocity)^2.

shown in Fig. 15. The steel rod penetrates the explosive at 10.6 mm/μs, and it forms a steady overdriven detonation wave moving at the same velocity as the steel rod, and with an overdriven effective C-J pressure of 90 GPa. The C-J pressure of PBX 9404 is 36.5 GPa and the C-J detonation velocity is 8.8 mm/μs. The calculation demonstrates that high-velocity jets cannot penetrate an explosive charge without initiating an overdriven propagating detonation.

When the rod penetration velocity becomes less than the C-J detonation velocity, the detonation wave moves away from the rod surface. To illustrate this, Fig. 16 shows density and mass fraction contours at 12 μs for a steel rod with an initial velocity of 5 mm/μs. Fig. 17 shows the pressure, density, and velocity along the z-axis at 12 μs. The steel rod penetrates the PBX 9404 at 3.2 mm/μs. The detonation wave proceeds at 8.7 mm/μs with a diverging effective C-J pressure of 35 GPa. The interface detonation product pressure is 15 GPa, which is 4.5 GPa greater than the ideal interface pressure at the rod tip of 10.5 GPa. As discussed in the previous section, the ideal model assumes that the pressure at zero particle velocity is zero, which is incorrect for constant volume detonation. A lower penetration velocity results than that expected from the ideal model.

The effect of the ~4-GPa additional interface pressure is most apparent when the rod velocity just suffices to cause prompt propagating detonation. The steel rod with an initial velocity of

1.5 mm/μs penetrates the explosive at 0.6 mm/μs, which is 0.4 mm/μs slower than it would penetrate inert PBX 9404. The steel rod interface pressure is 5.0 GPa, which is ~4 GPa higher than the 0.9-GPa ideal interface pressure. Illustrating the importance of this increased interface pressure upon penetration velocity, the calculated penetration velocity is about the same for the 0.7-mm/μs steel rod, where the explosive does not decompose, as for the 1.5-mm/μs rod, where the explosive detonates.

CONCLUSIONS

1. For engineering purposes, the initial jet penetration velocity into an inert substance can be estimated, using the shock impedance relationships ($V_j/V_p = 1 + \rho_t U_{st}/\rho_j U_{sj}$ and $P = \rho_t U_{st} V_p$). Final penetration velocity can be estimated, using Bernoulli's theorem ($V_j/V_p = 1 + \sqrt{\rho_t/\rho_j}$). The interface pressure, P, at the jet tip is estimated using $P = \frac{1}{2} \rho_t V_p^2$.

2. The calculated penetration velocity into explosives that are initiated by low-velocity jets is significantly less than for nonreactive solids of the same density. Reaction products near the jet tip have a higher pressure than in inert materials of the same density, and thus impede the jet penetration. The effect is less important as the jet velocities increase. Thus when the target is a high explosive, the Bernoulli equation needs an additional term, p^*, $[\frac{1}{2} \rho_j (V_j - V_p)^2 = \frac{1}{2} \rho_t V_p^2 + p^*)]$, where p^* is approximately 4.0 GPa for the explosives studied.

3. The critical jet or projectile velocity for initiating propagating detonation can be estimated using the projectile diameter and the Held critical V^2d expression. In PBX 9502, the jets initiate an overdriven detonation smaller than the critical diameter, which either fails or enlarges to greater than the critical diameter while the overdriven detonation decays to the C-J state. In PBX 9404, the jet initiates a detonation that propagates only if it is maintained by the jet for an interval sufficient to establish a stable curved detonation front. A critical expression independent of the projectile material is $\rho V^2 d$, where ρ is the projectile density.

4. The above methods are approximate. If jet or projectile velocity is not substantially constant, or if the projectile length is not much greater than the diameter, numerical calculations will be necessary. The Held criterion may be useful even when the projectile length is the same as the diameter.

5. A jet with a penetration velocity greater than the C-J detonation velocity of the target explosive gives an overdriven detonation wave proceeding ahead of the jet with a velocity near that of the jet.

6. If the jet diameter and velocity histories are known, all the experimentally observed jet penetration behavior of metals or explosives can be modeled numerically. Also, if the jet or projectile length is known, the penetration depth and hole diameter may be calculated.

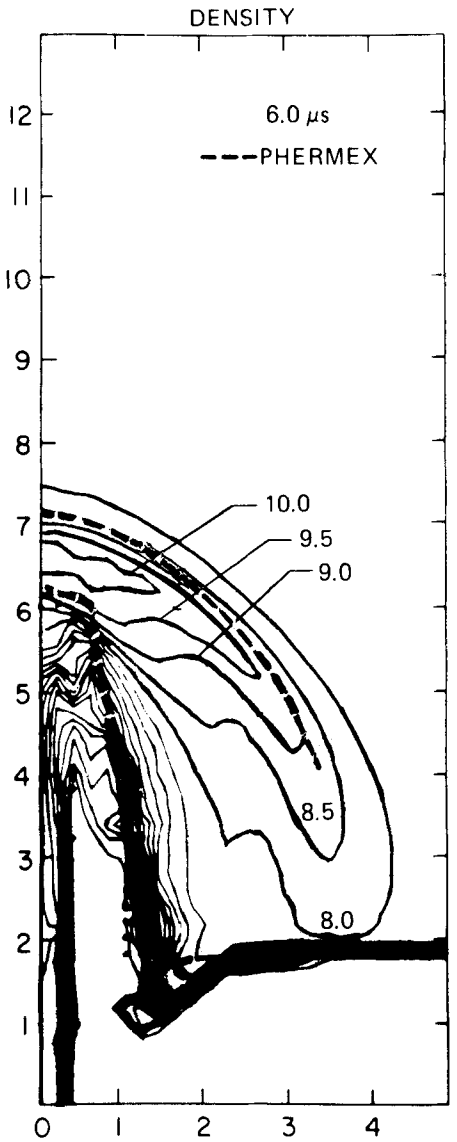

FIGURE 1
Calculated density profiles after 6.0 μs of penetration of a steel block 110 mm long and 50 mm wide, by an 8.0-mm-thick steel jet moving with a tip velocity that has decreased to 12 mm/μs from the initial velocity of 18 mm/μs. The experimental shock front profile and target interface are shown as dashed lines. The jet has penetrated 45 mm of steel. The density contour interval is 0.5 mg/mm^3.

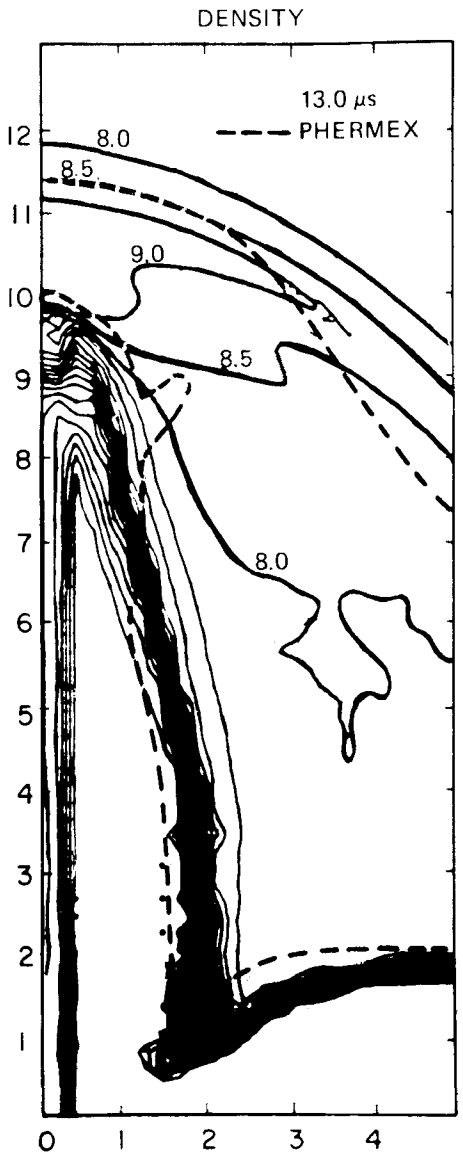

FIGURE 2

Calculated density profiles after 13 μs of penetration of a steel block 110 mm long by 50 mm wide, by an 8.0-mm-thick steel jet moving with tip velocity that has decreased to 7.75 mm/μs from the initial velocity of 18 mm/μs. The experimental shock front profile and target interface are shown as dashed lines. The jet has penetrated 80 mm of steel. The density contour interval is 0.5 mg/mm^3.

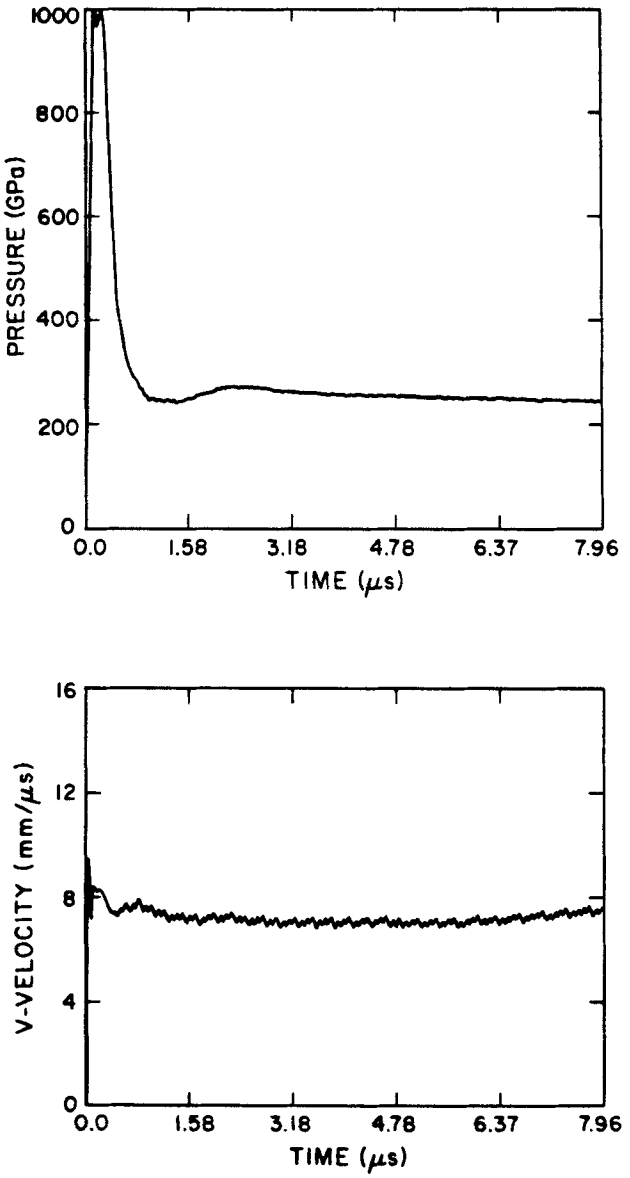

FIGURE 3
Calculated pressure and velocity at the interface between the advancing steel rod tip (whose initial velocity was 15 mm/μs) and the target are shown as functions of time.

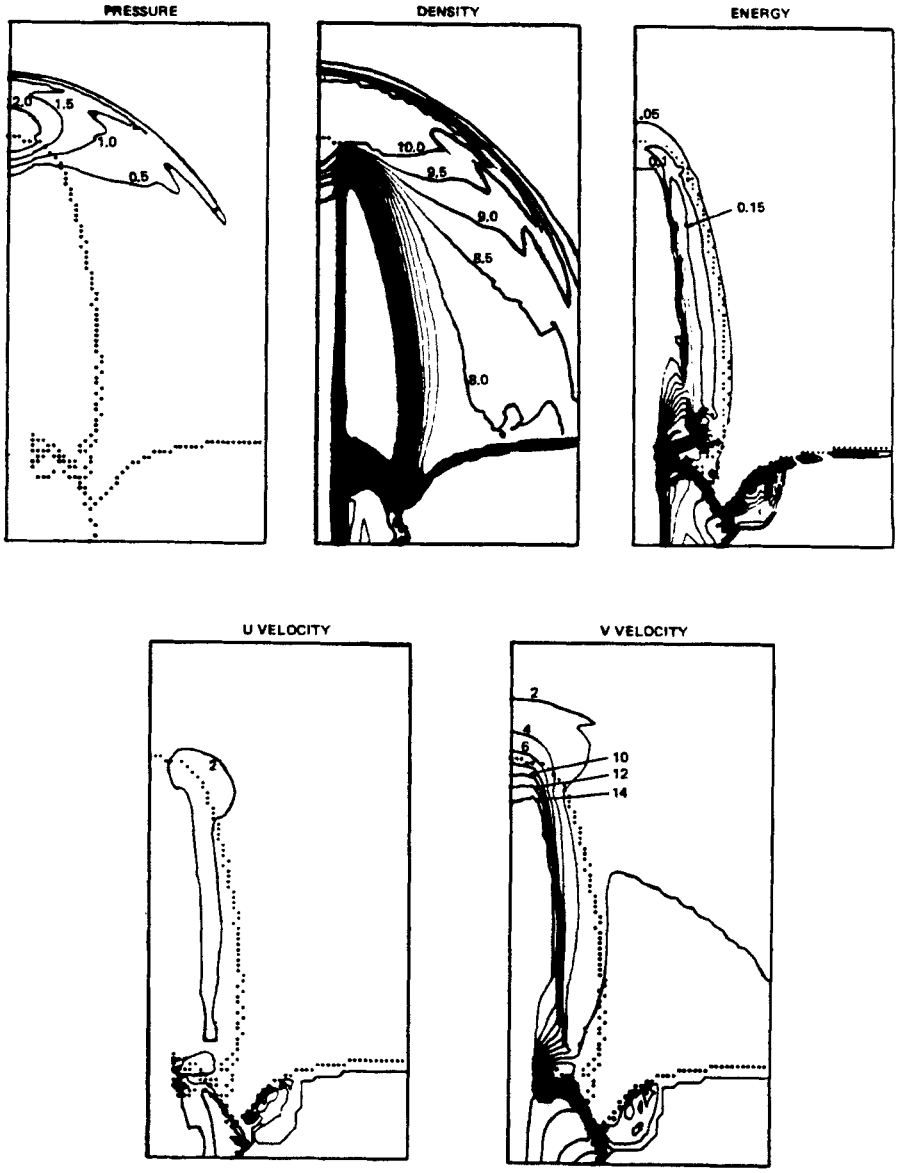

FIGURE 4

Pressure, density, energy, and horizontal (U) and vertical (V) velocity contours at 8.0 μs for a steel rod with a 15-mm/μs initial velocity penetrating a steel target. The pressure contour interval is 50 GPa, the density contour interval is 0.5 mg/mm^3, the energy contour interval is 0.05 Mbar · cm^3/g, and the velocity contour interval is 2 mm/μs. The graph is 50 mm wide and 100 mm high.

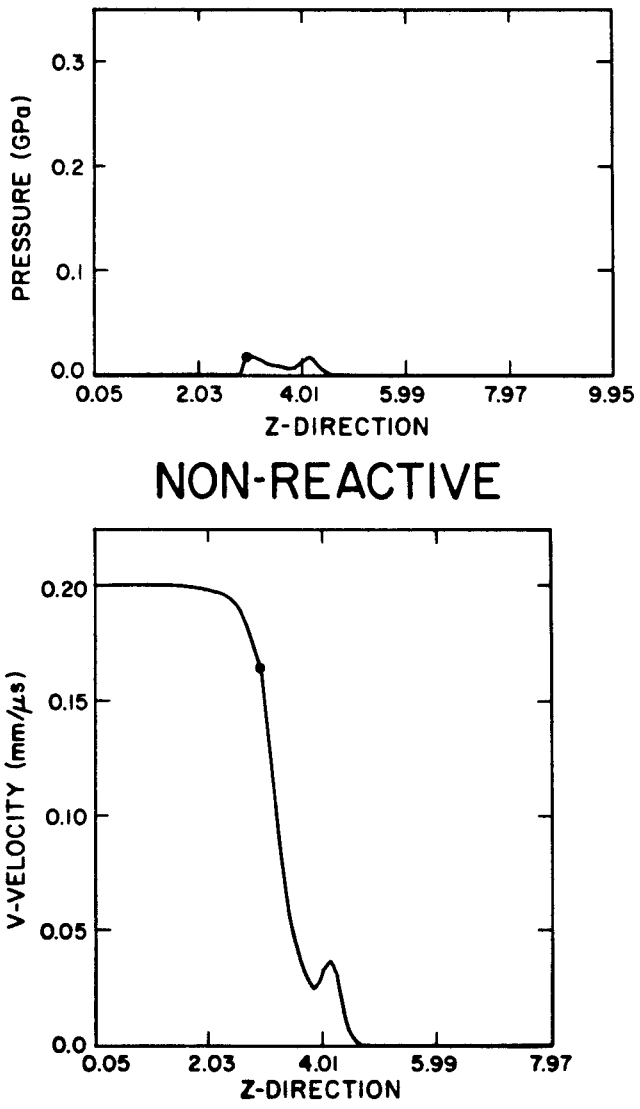

FIGURE 5, PART 1

Calculated one-dimensional graphs near the axis of the tantalum rod (with a 2.0-mm/μs initial velocity) for a Composition B target, with and without reaction, after 6.0 μs. The interface is shown by a star.

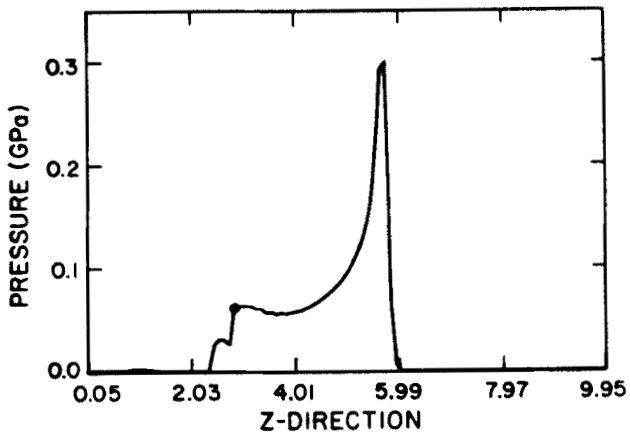

REACTIVE

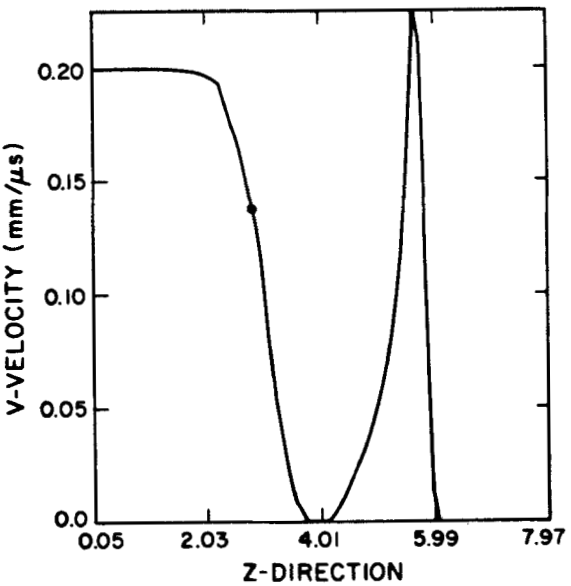

FIGURE 5, PART 2

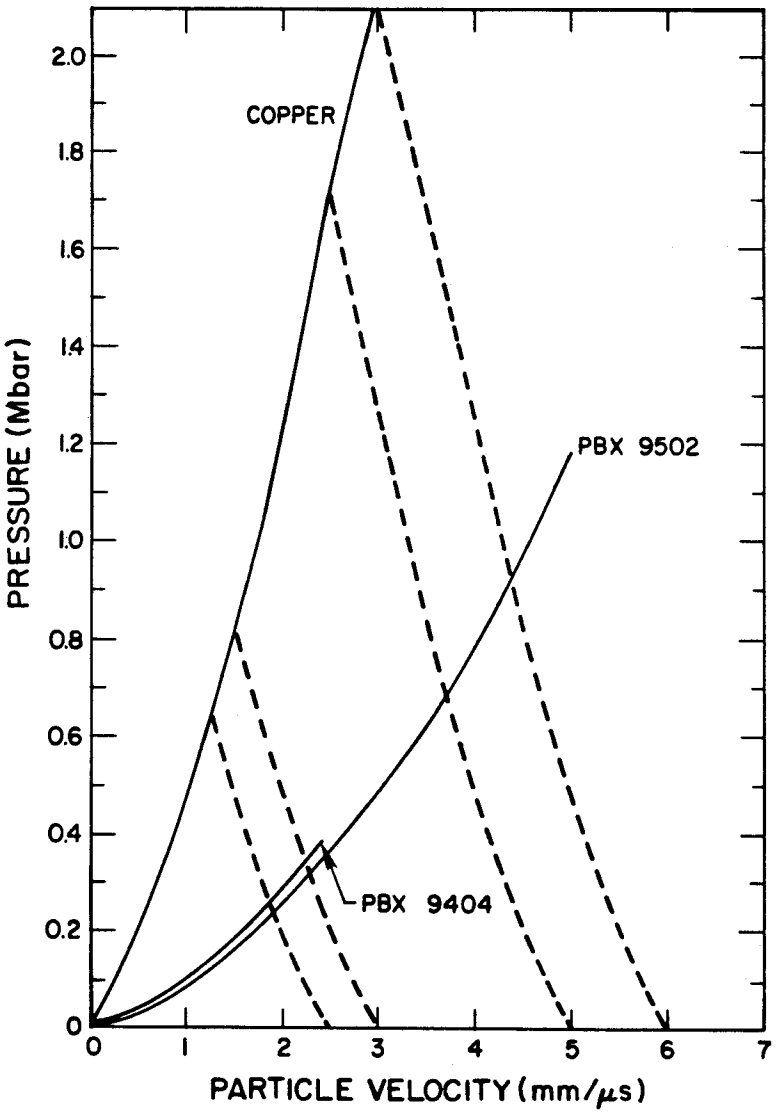

FIGURE 6
The pressure-particle velocity Hugoniots for copper, PBX 9502, and PBX 9404 with the reflected shock states for copper with initial free-surface velocities of 6.0, 5.0, 3.0, and 2.5 mm/μs.

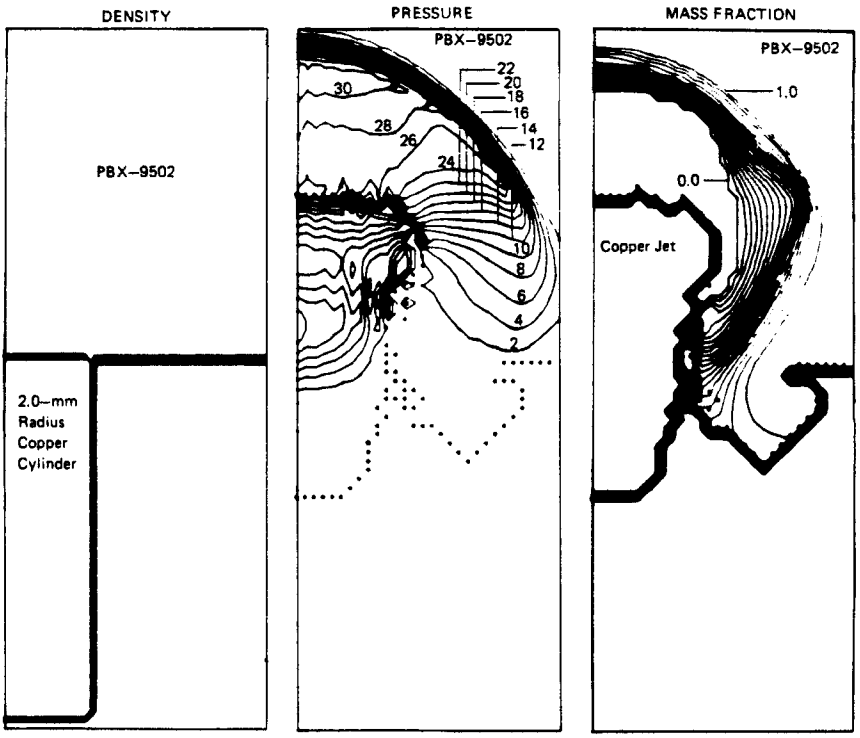

FIGURE 7

The initial density profile and the pressure and mass fraction profiles for a 4-mm-diameter copper cylinder of 7.0 mm/μs shocking PBX 9502 at 0.75 μs. The isobar contour interval is 2 GPa and the mass fraction contour is 0.05. The graph is 6 mm wide and 6 mm high.

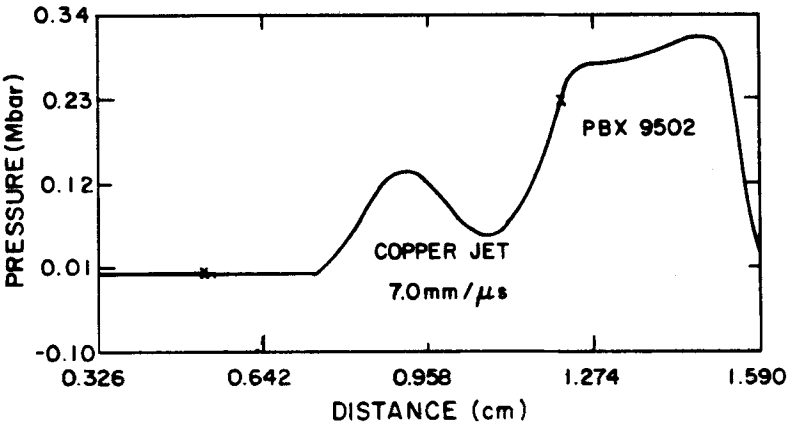

FIGURE 8
The pressure profile along the axis is shown for a 4-mm-diameter copper cylinder of 7.0 mm/μs shocking PBX 9502 at 0.75 μs.

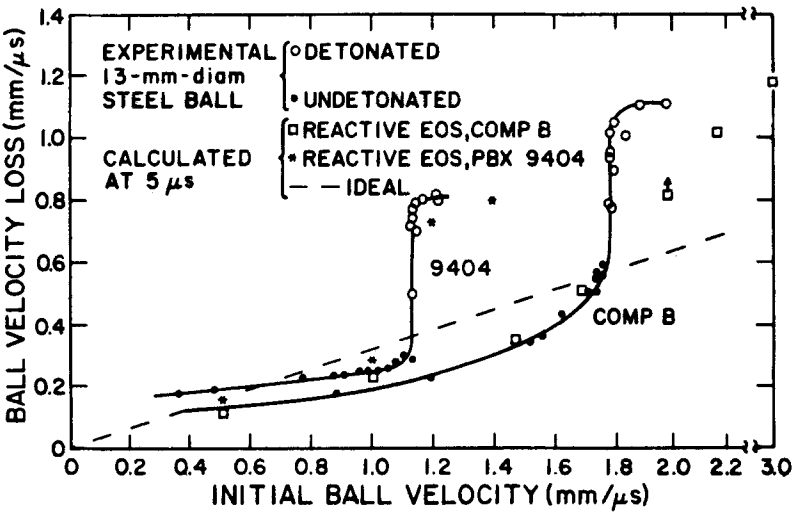

FIGURE 9
Initial ball velocity vs the ball velocity loss for a 13-mm-diameter steel ball penetrating PBX 9404 or Composition B-3.

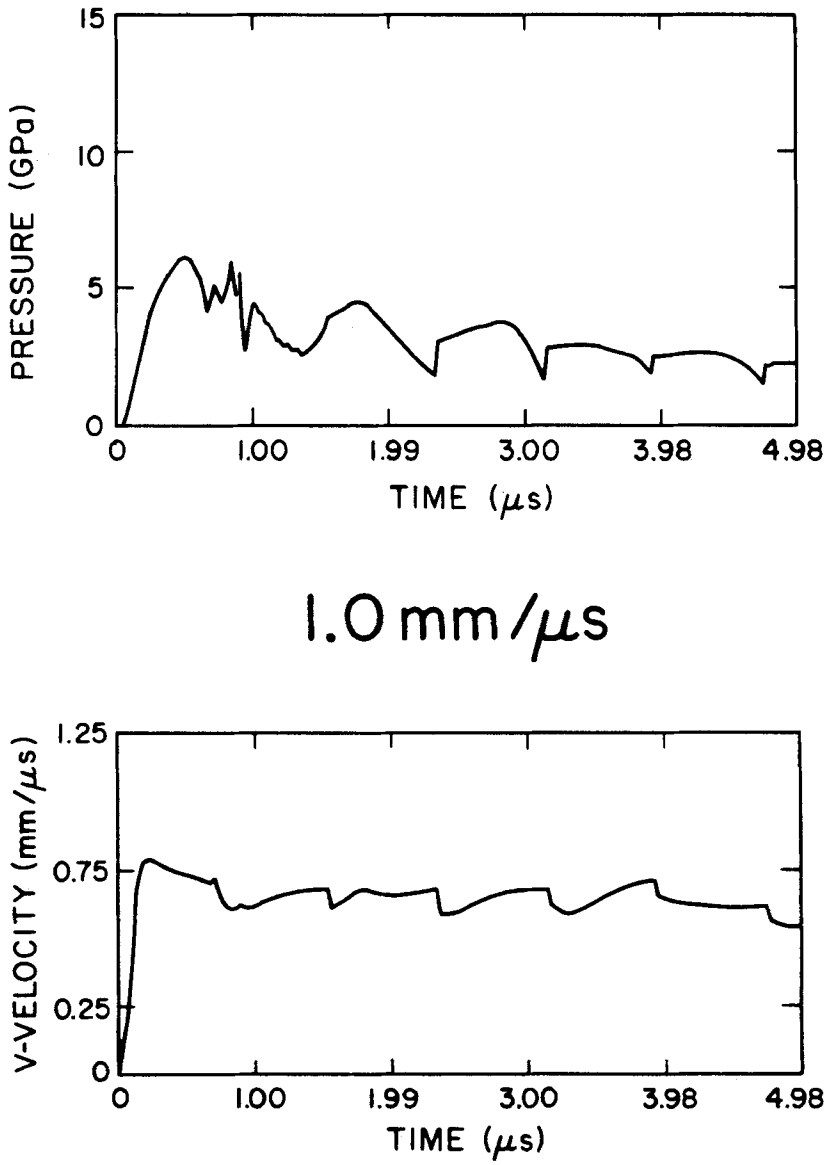

FIGURE 10, PART 1

Axial interface pressure and velocity as functions of time between a steel ball (initially moving at 1.2 or 1.0 mm/μs) and a PBX-9404 target. The 1.0-mm/μs ball velocity is too slow to cause prompt propagating detonation, whereas the 1.2-mm/μs ball does result in a propagating detonation.

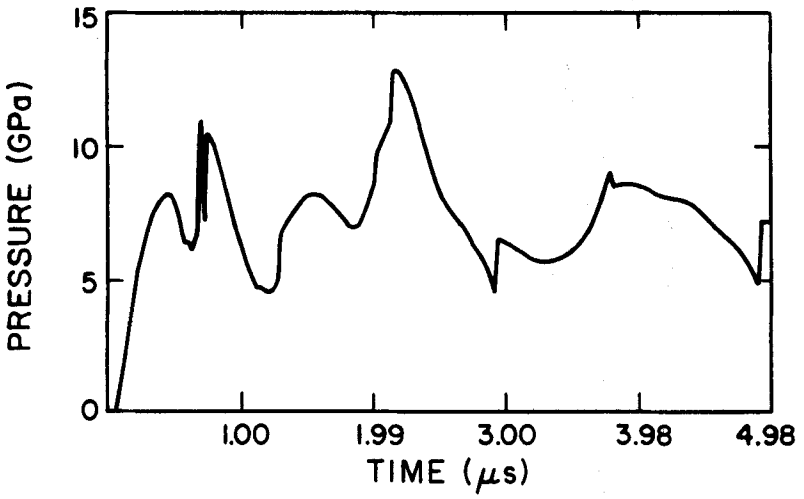

1.2 mm/μs

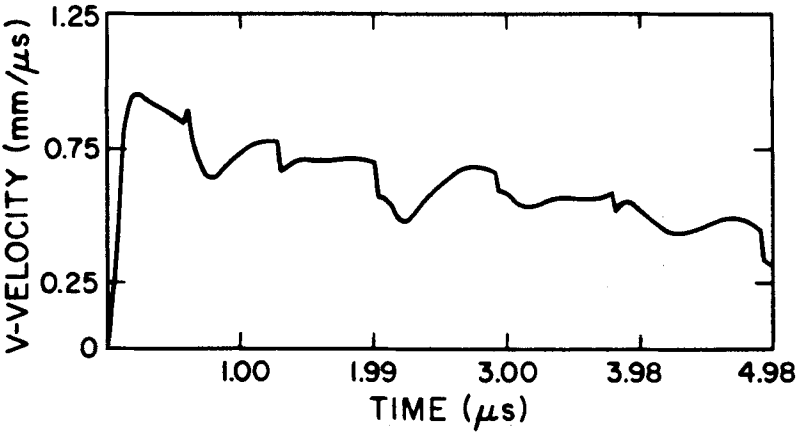

FIGURE 10, PART 2

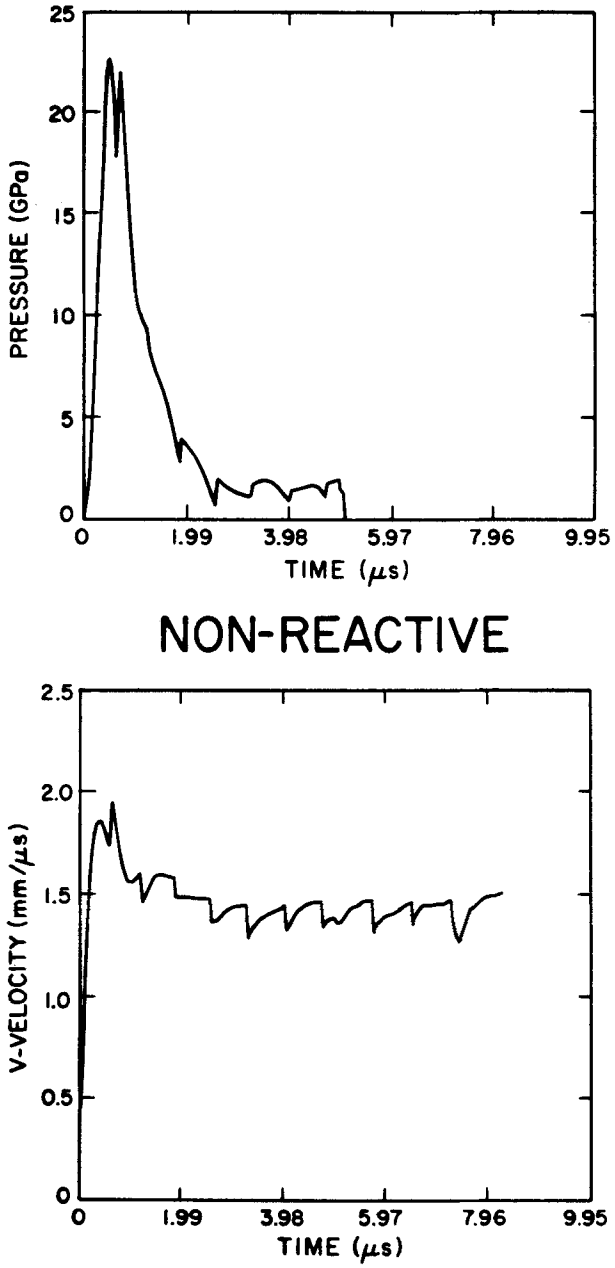

FIGURE 11, PART 1
Interface pressure and velocity at the tip of a 6.5-mm-radius steel rod initially moving at 2.0 mm/μs into reactive and non-reactive Composition B.

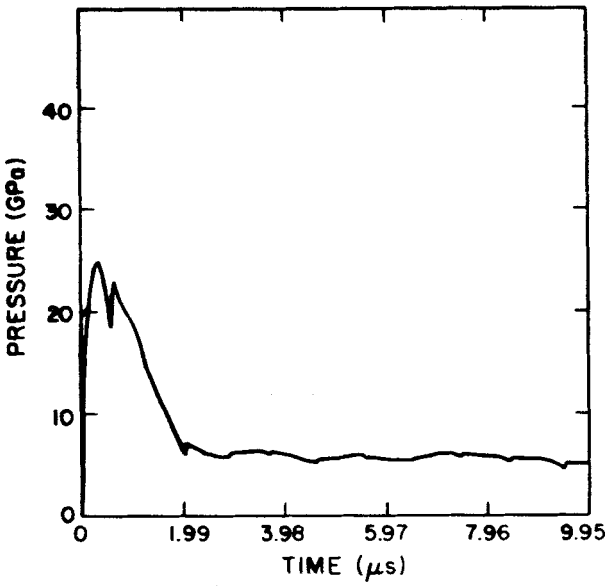

REACTIVE

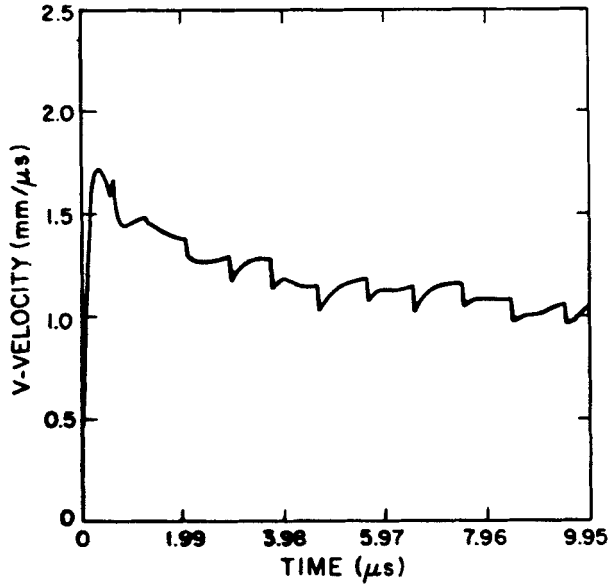

FIGURE 11, PART 2

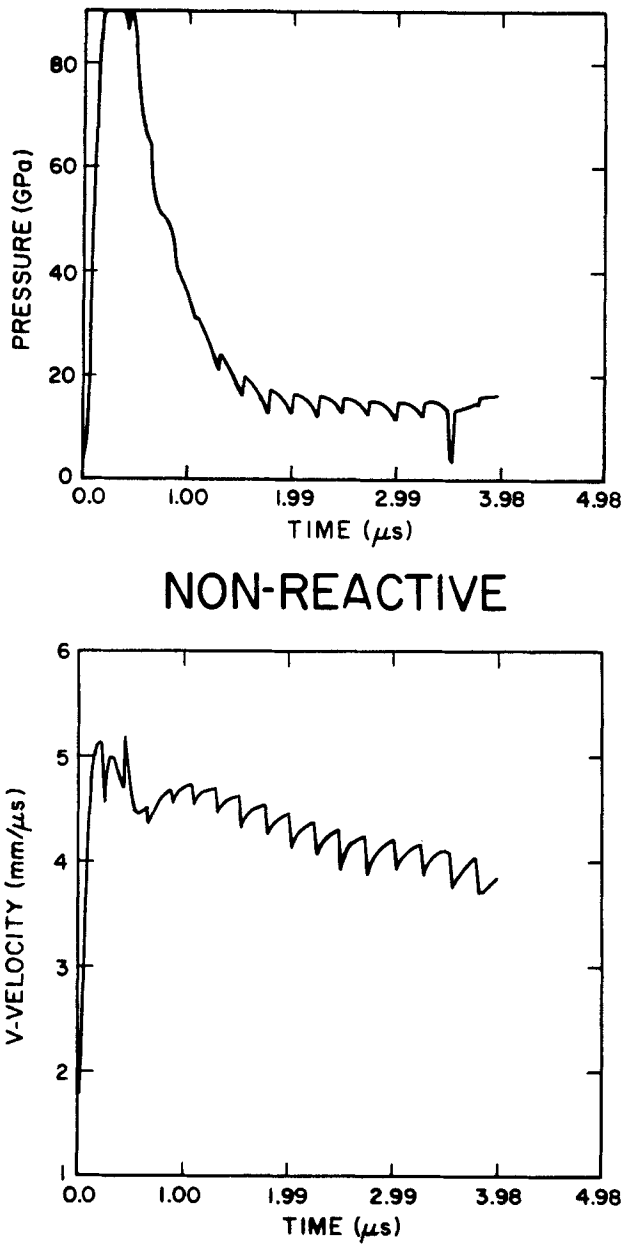

FIGURE 12, PART 1
Interface pressure and velocity at the tip of a 6.5-mm-radius steel rod initially moving at 6.0 mm/μs penetrating reactive and nonreactive Composition B.

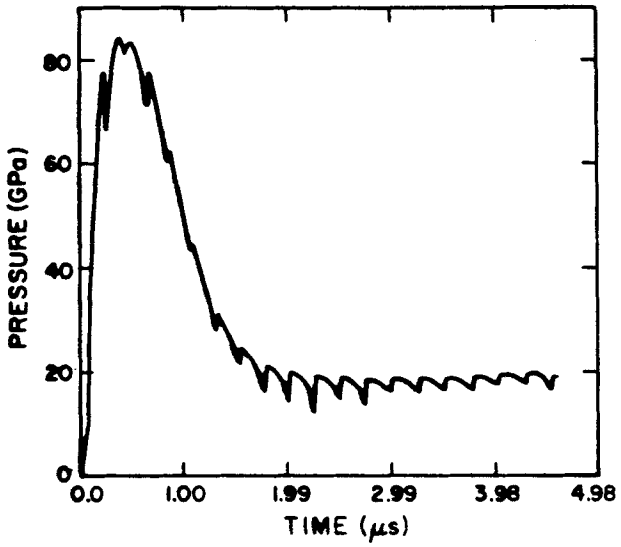

REACTIVE

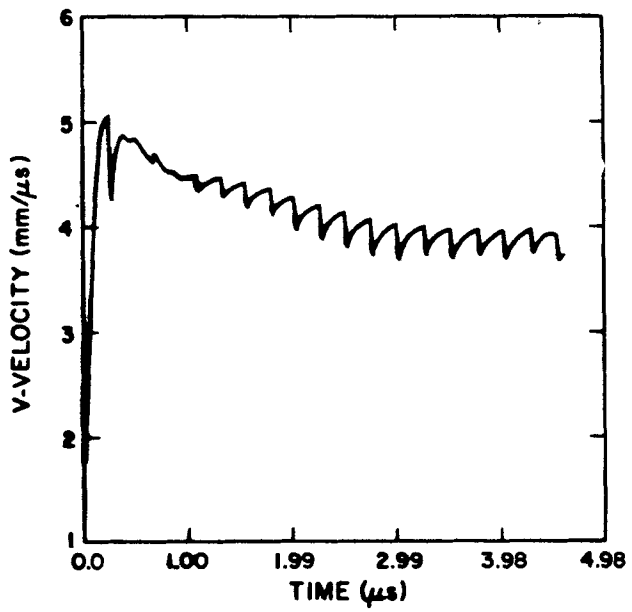

FIGURE 12, PART 2

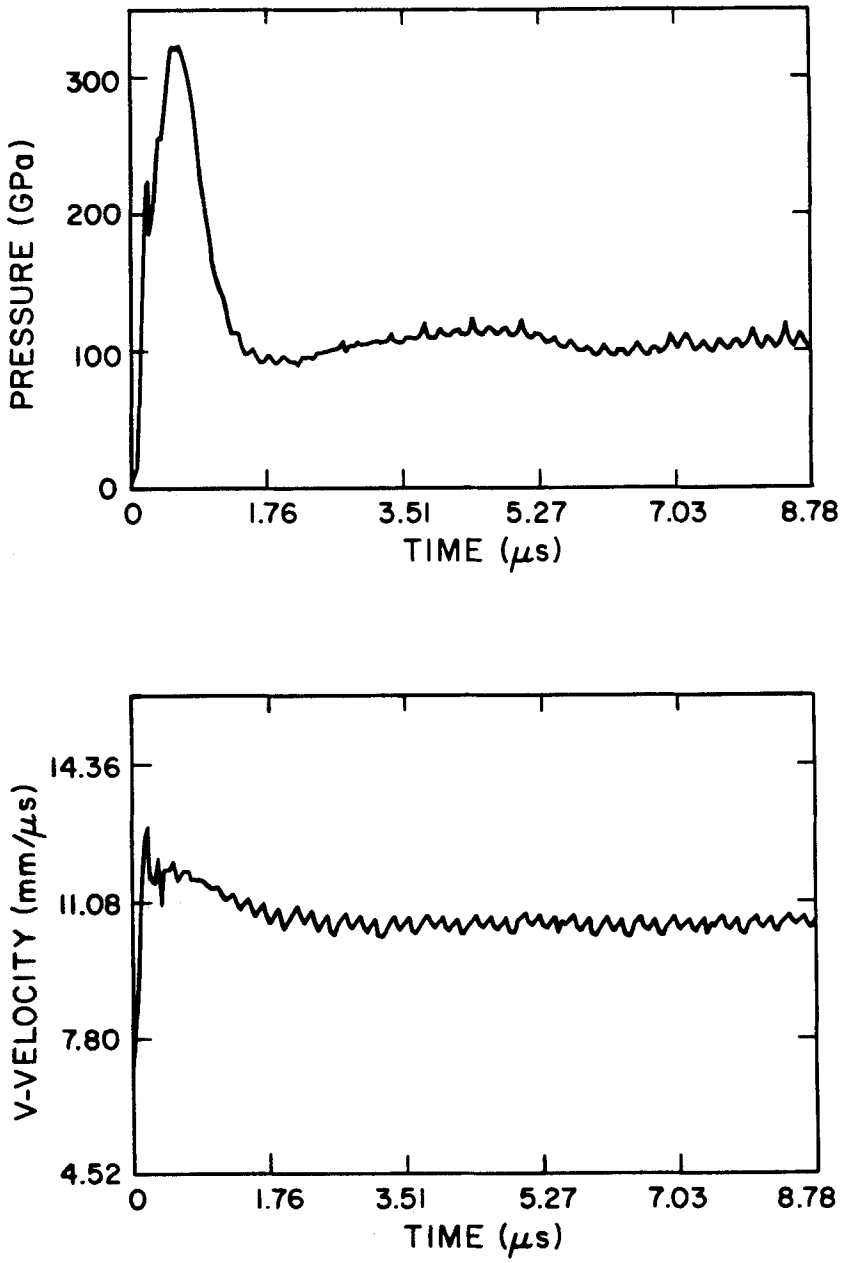

FIGURE 13
Interface pressure and velocity at the tip of a 16-mm-diameter steel rod initially moving at 15 mm/μs penetrating PBX 9404.

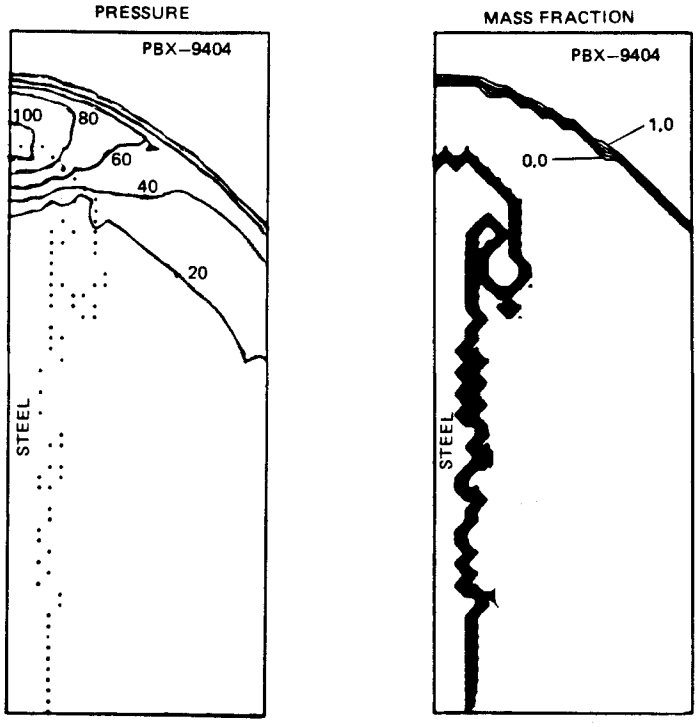

FIGURE 14
Pressure and mass-fraction contours at 8.8 μs, for a 16-mm-diameter steel rod initially moving at 15 mm/μs penetrating PBX 9404. The pressure contour interval is 20 GPa, the mass fraction interval is 0.2. The graph is 50 mm wide and 130 mm high.

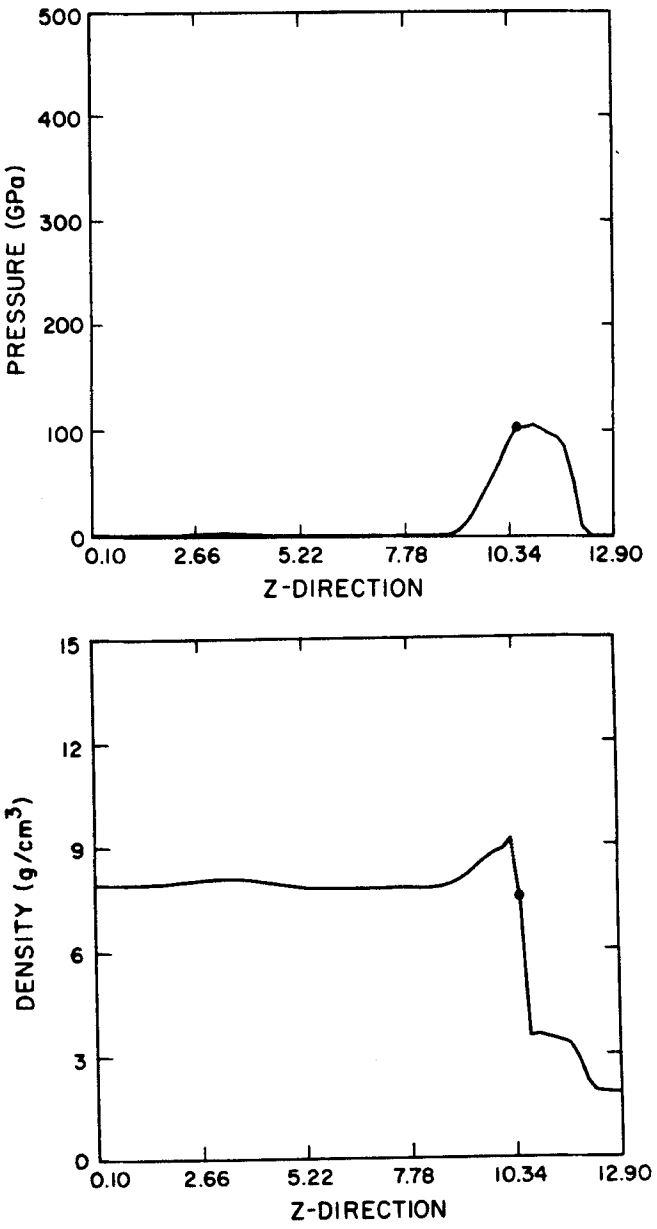

FIGURE 15, PART 1
Pressure, density, and velocity one-dimensional graphs, along and near the vertical z-axis, at 8.8 μs, for a 16-mm-diameter steel rod initially moving at 15 mm/μs penetrating PBX 9404.

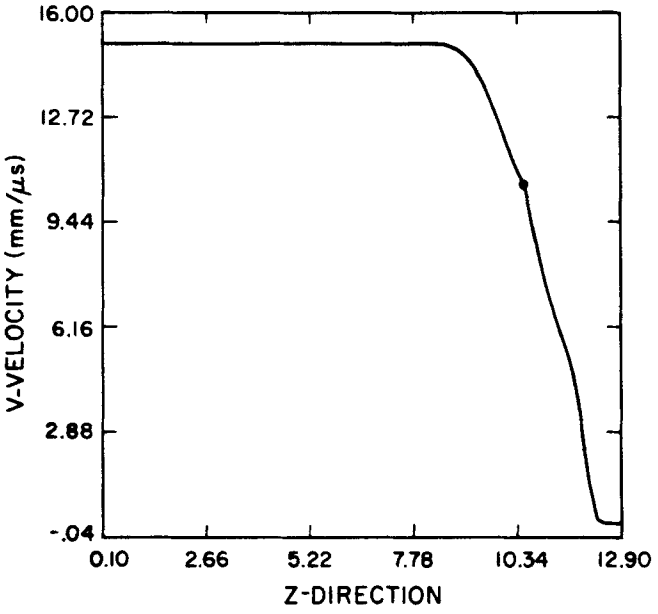

FIGURE 15, PART 2

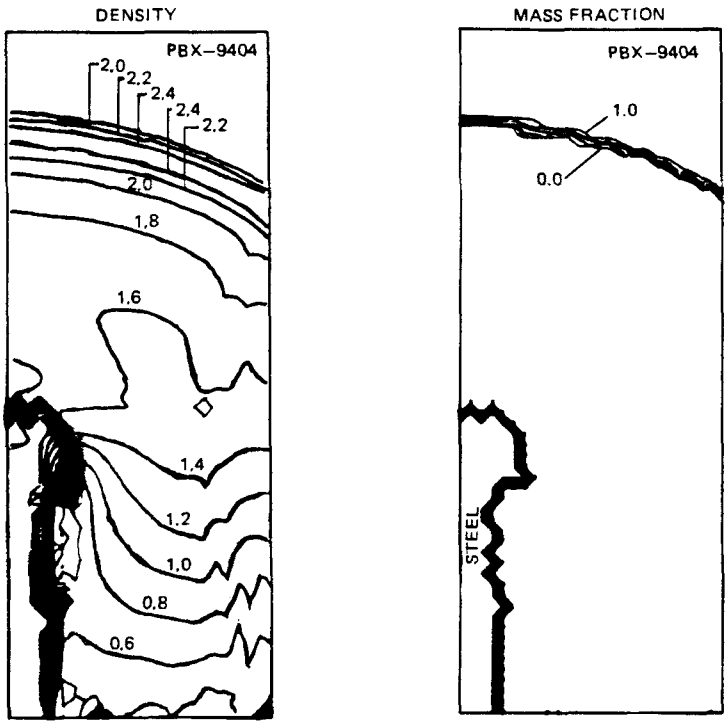

FIGURE 16

Density and mass fraction contours at 12.0 μs, for a 16-mm-diameter steel rod initially moving at 5 mm/μs penetrating PBX 9404. The density contour interval is 0.2 mg/mm^3 and the mass fraction interval is 0.2. The graph is 50 mm wide and 130 mm high.

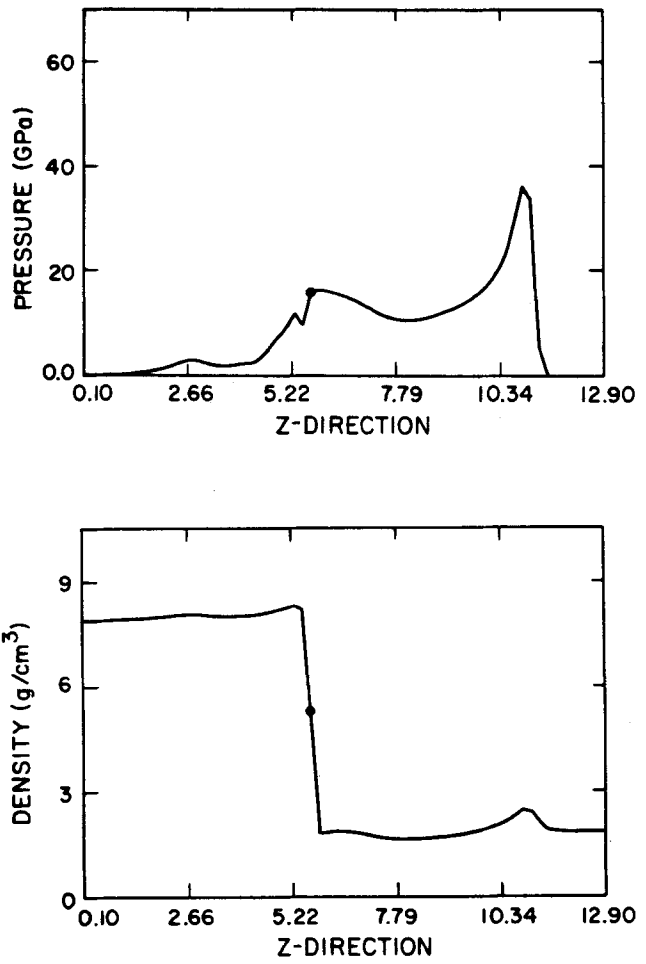

FIGURE 17, PART 1
Pressure, density, and velocity one-dimensional graphs along and near the vertical z-axis at 12.0 μs, for a 16-mm-diameter steel rod initially moving at 5 mm/μs penetrating PBX 9404.

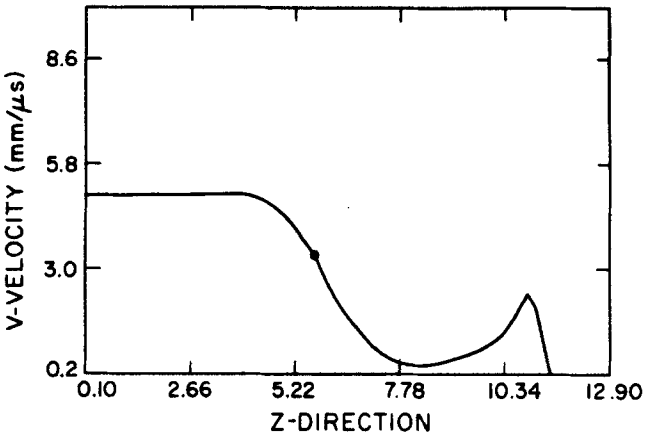

FIGURE 17, PART 2

ACKNOWLEDGMENTS

The authors gratefully acknowledge the contributions of Arthur W. Campbell, Lawrence W. Hantel, Allen L. Bowman, James D. Kershner, Charles A. Forest, Charles W. Mautz, and Donald L. Upham of the Los Alamos National Laboratory; Mansfred Held, MBB-Schrobenhausen, West Germany; and Norris E. Hoskin, AWRE, and Peter R. Lee, RARDE, England.

REFERENCES

1. Garrett Birkhoff, Duncan P. MacDougall, Emerson M. Pugh, and Sir Geoffrey Taylor, "Explosives with Lined Cavities," J. App. Phys. 19, 563-582 (1948).
2. M. Held, "Initiating of Explosives, A Multiple Problem of the Physics of Detonation," Explosivstoffe, Vol. 5, pp. 98-113 (1968).
3. M. H. Rice, "Penetration of High Explosives by Inert Projectiles," Systems, Science and Software report SS-R-78-3512 (1977).
4. Wallace E. Johnson, "Three-Dimensional Computations in Penetrator-Target Interactions," Ballistic Research Laboratory report BRL-CR-338 (1977).
5. Charles L. Mader, Numerical Modeling of Detonations, University of California Press, Berkeley, 1979.
6. Charles L. Mader, LASL PHERMEX Data, Vol. III, University of California Press, Berkeley, 1980.

7. Charles L. Mader and Milton Samuel Shaw, "User's Manual for SIN," Los Alamos Scientific Laboratory report LA-7264-M (September 1978).

8. Arthur W. Campbell and Lawrence W. Hantel, Los Alamos National Laboratory, private communication.

This paper was developed under the auspices of the U.S. Department of Energy.